Taylor & Francis
Taylor & Francis Group

Automatika

Journal for Control, Measurement, Electronics, Computing and Communications

ISSN: (Print) (Online) Journal homepage: https://www.tandfonline.com/loi/taut20

Enhancing LVRT capability of DFIG using cooperative control of BTFCL and RPC

K. Gireeshma & S. Chandramohan

To cite this article: K. Gireeshma & S. Chandramohan (2023) Enhancing LVRT capability of DFIG using cooperative control of BTFCL and RPC, Automatika, 64:1, 51-62, DOI: 10.1080/00051144.2022.2098108

To link to this article: https://doi.org/10.1080/00051144.2022.2098108

Published online: 14 Jul 2022.

AUTOMATIKA
2023, VOL. 64, NO. 1, 51–62
https://doi.org/10.1080/00051144.2022.2098108

REGULAR PAPER

OPEN ACCESS Check for updates

Enhancing LVRT capability of DFIG using cooperative control of BTFCL and RPC

K. Gireeshma and S. Chandramohan

Department of Electrical engineering, Anna University, Chennai, India

ABSTRACT

To integrate the high penetration of power from wind farms into a grid, one of the key requirements posed by new grid codes is Low Voltage Ride Through (LVRT) capability. This paper studies voltage compensation-based methods to improve fault ride-through capability of the grid-connected Doubly Fed Induction Generator (DFIG). Bridge Type Fault Current Limiter (BTFCL) and Reactive Power Control (RPC), which is acting as an active voltage compensator, are cooperatively controlled in this study to achieve better LVRT capability of DFIG. Additionally, the design considerations to select shunt impedance of BTFCL are described to get optimal performance of the system under consideration. The test system was modelled and simulated in MATLAB/SIMULINK environment. The effectiveness of the proposed method is tested by comparing it with the conventional Crowbar resistance method. Simulation results show that the cooperative control of self-acting BTFCL and an intelligent RPC can effectively reduce the fault current, improves the stator voltage of DFIG for continuous operation and provides reactive power support to the grid during fault conditions.

ARTICLE HISTORY
Received 21 July 2021
Accepted 1 July 2022

KEYWORDS
Low voltage ride-through capability; bridge type fault current limiter; reactive power control; doubly fed induction generator; renewable energy integration; crowbar resistance

1. Introduction

The demand for electric power increases very rapidly in recent years, to meet this demand; available conventional sources are very finite and take more time to regenerate. One of the major problems with these fossil fuels is their CO_2 emissions while generating power. According to International Energy Agency (IEA) the power sector's CO_2 emissions are equal to 40% of global CO_2 emissions [1] in 2018. To overcome the above-mentioned problems, the government and people are focusing more on non-conventional energy sources such as wind, solar, biomass, etc. Among all sustainable energy sources, wind power is gaining importance as it is a technically and economically proven reliable source to produce electricity.

The present total wind power installed capacity is 743 GW [2], according to Global Wind Energy Council (GWEC) by 2050, this is planned to increase by 3300 GW [3]. As the penetration of power from wind energy increases, the major concern is to maintain stability of the grid. LVRT is one of the most promising solutions to maintain stability in this scenario. The new grid codes made it compulsory that all installed wind plants and upcoming ones must have LVRT capability [4].

DFIGs are occupying a large portion (50%) of the wind power market [5] due to their lightweight, low cost, small size, low rated (25% to 50% of generator rating) power converters and independent control of real and reactive power. While an increasing portion of power from wind sources, the DFIGs fail to satisfy new grid codes because of very low LVRT capability. As one of the converters of DFIG is directly connected to the grid, these generators are very much sensitive to faults suach as voltage dips and voltage swells. To attract the owners of wind power and to meet new grid code requirements, it is very much necessary to improve the LVRT capability of DFIG.

Any voltage sag that occurs at the Point of Common Coupling (PCC) of a DFIG-based wind plant can cause very high fault current flows through Rotor Side Converter (RSC) which may damage the low-rated power electronic switches, large fluctuations in DC link voltage waveform and electromagnetic torque oscillations. This may reduce the lifetime of the turbine shaft and gearbox and also the reliability of the machine.

Several methods [6] are available in the literature to enhance the LVRT capability of DFIG-based wind plants. From the literature, it is observed that the available methods are divided into two categories [7] namely: (1) External hardware protection-based methods and (2) Internal modification-based methods. The internal modification-based methods include the modified vector control method proposed in [8] where the inner current control loop is changed to sliding mode control and controller gains are chosen using a positive semi-definite barrier function. A negative sequence current compensation technique is discussed in [9] to reduce the rotor over-current and smoothen the electromagnetic torque and reactive power during the

CONTACT Gireeshma K gireeshmaeee253@gmail.com Anna University, Chennai 600025, India

asymmetrical faults. Dual-loop control is proposed in [10] in which an additional control loop in combination with the traditional current control loop is proposed to account for transient stator flux, thereby controlling active, reactive powers and reducing rotor over current.

Feed forward rotor current is additionally added to RSC for better tracking of rotor current compared with conventional PI controllers as discussed in [11]. Another common method is to modify the converter control structure to participate in Transient Voltage Control (TVC) [12,13], but TVC alone is not sufficient to boost PCC voltage during the worst situations like very low stator voltage due to faults. A dynamic coordination control strategy, which is based on the calculation of maximum available reactive power, was proposed in [14], to enhance the reactive power capability of DFIG, but without any fault current limitation. An improved fault ride-through system for DFIG, based on stator voltage control by modification of both the converters is discussed in [15].

The control structure of DFIG itself is a bit complex, these internal modification-based methods make it a more complex structure, and hence the external protection-based methods are gaining importance because of their simple control. The most discussed external protection-based method in the literature is Crowbar [16–19]-based resistance connected in series with RSC to limit the fault current. A modified DC chopper was proposed in [20] to not only maintain the DC link voltage at a constant level but also to reduce the fault current through the rotor and stator of DFIG.

Inserting a series resistance into the generator circuit using a Series Dynamic Breaking Resistor (SDBR) was described in [21] to enhance the Fault Ride Through (FRT) capability. A Dynamic Voltage Restorer (DVR) combined with an inductive fault current limiter was proposed in [22] to maintain the stable voltage and to limit the rotor over current during the faults on the grid. Superconducting Magnetic Energy Storage (SMES) is used to maintain the grid stability during small and large disturbances by considering the exact location and ratings of SMES discussed in [23]. A new method gaining importance in recent days is Superconducting Fault Current Limiter (SFCL) combined with SMES to enhance the LVRT capability was discussed in [24,25] however with the very high installation cost. Resistive type SFCL conceptual design and evaluation were discussed in [26] to enhance the LVRT of DFIG. SMES and DVR are controlled combination to enhance the LVRT of DFIG was discussed in [27]. Unified Power Quality Conditioner (UPQC)-based energy storage was proposed in [28] to enhance the LVRT of DFIG and to reduce the oscillations during asymmetrical faults thereby improving the stability of the grid. Combined control of Resistive type SFCL and SMES was discussed in [29] for LVRT enhancement of DFIG but without any reactive power support from DFIG. A Modified Bridge-Resistive-type Superconducting Fault Current Limiter (MBR-SFCL) was proposed in [30], to enhance the LVRT capability of DFIG and compared the proposed method with conventional SFCL, but without any reactive power support from DFIG during the fault.

A new device with a lot of applications in power systems and excellent fault current limiting properties is Bridge Type Fault Current Limiter (BTFCL) [31,32]. To improve the transient stability and to enhance the LVRT capability of DFIG during the fault conditions, the authors proposed the Fuzzy logic-based Capacitive Bridge Fault Current Limiter (CBFCL) in [33], this proposed fault current limiter is used to reduce the voltage drop by generating the instantaneous reactive power during the fault conditions.

BTFCL is used to enhance the transient stability of DFIG in [34], but with BTFCL alone, DFIG is failed to provide any reactive power support to boost the PCC voltage. The key contributions of this paper are as follows.

- A lot of pieces of literature are available to limit the fault current of DFIG but only a few authors discussed providing reactive power support.
- In this paper authors propose the cooperative control of BTFCL and Reactive Power Control (RPC), to limit the fault current and provide reactive power support from DFIG to the grid.
- There by successfully achieving the two main requirements of LVRT capability as per new grid codes.

The organization of this paper is as follows. The importance of LVRT requirements is explained in Section 2, the basic cooperative principle is described in Section 3, modelling and analysis of DFIG, BTFCL, RPC, design considerations for BTFCL, PI controllers and Crowbar method are described in Section 4, simulation results were presented and analyzed in Section 5 and the findings of the study are concluded in Section 6.

2. Importance of LVRT requirements

The installed capacity of wind power has been increasing rapidly over the past 10 years and the cumulative wind power installed up to 2020 is 743 GW. According to the Global Wind Energy Council (GWEC) this may increase and supply up to 30% of total world electric power by 2030, which means it reduces 3.3 billion tones of CO_2 emissions by the end of 2030 [35].

Integrating such a large amount of wind power into the grid poses critical challenges using grid stability and security. The previous grid codes are allowed to disconnect the wind plant during faults and low voltage situations [36]. But during large penetration from wind source, a sudden disconnection of wind plant may

raise the severity of the fault and leads to totally unstable operation of the grid. Hence countries around the world are forced to develop new grid codes by mandating LVRT capability for all upcoming and already installed wind plants [36].

LVRT requires mainly two objectives [36] i.e. (1) During a fault, the wind unit needs to continue its operation with the grid for a specific period before it is allowed to be disconnected, as shown in Figure 1 and (2) To bring power system back to its normal operation, wind unit needs to provide reactive power support to the grid, as shown in Figure 2.

3. Basic cooperative principle

Figure 3 shows the 9 MW wind plant formed by 6 wind turbines with a capacity of 1.5 MW each and it is connected to PCC through a step-up transformer T_1, which feeds power to the 220 kV grid through a 30 km

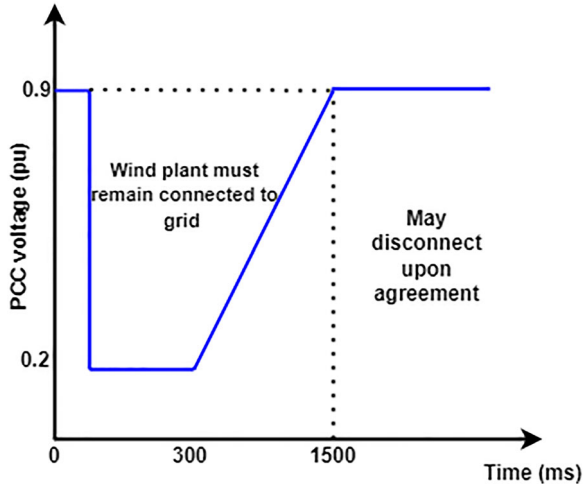

Figure 1. Voltage requirement curve of LVRT [36].

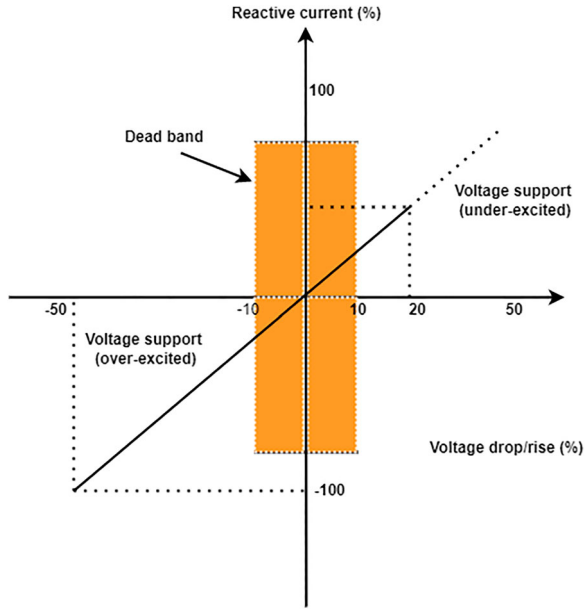

Figure 2. Reactive power requirement curve of LVRT [36].

double circuit line and transformer T_2. The proposed BTFCL is connected in series with the transmission line (T_{r2}). The parameters of DIFG used in this study are listed in Table 1. RSC and GSC can be controlled within their available rating [37–40] such that DFIG can contribute reactive power support to the grid. The reactive power output of the DFIG stator and the reactive power exchange between GSC to the grid is given by [41]

$$Q_{stator} = \frac{3}{2}(V_{qs}i_{ds} - V_{ds}i_{qs}) \tag{1}$$

$$Q_g = \frac{3}{2}(V_{qg}i_{dg} - V_{dg}i_{qg}) \tag{2}$$

where v, i represent voltage, current and subscripts s, g, d and q represent stator, grid, direct and quadrature axis components. After applying stator flux oriented synchronously rotating reference frame [41] with stator flux is aligned with d-axis to equation (1) results in the following

$$Q_{stator} = \frac{3}{2}|V_s i_{qs}| \tag{3}$$

After applying synchronously rotating reference frame [41], with grid voltage is aligned with d-axis to equation (2) results in the following

$$Q_g = \frac{3}{2}|V_s i_{qg}| \tag{4}$$

From equations (3) and (4), it is seen that magnitude of reactive power output from DFIG depends on the post fault stator voltage V_s, which means Reactive Power Control (RPC) acts like an active voltage compensator. Stator reactive power can be controlled by controlling

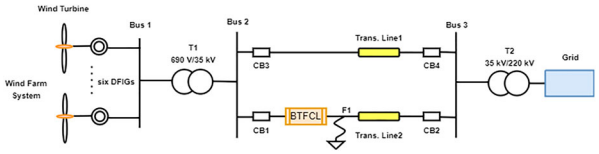

Figure 3. Schematic diagram of 9 MW DFIG wind farm with bridge-type fault current limiter.

Table 1. Parameters of DFIG under study.

Parameter	Value
Base power	10 MVA
Nominal power	9 MW
Stator voltage (rms)	690 V
Rotor voltage (rms)	1975 V
Stator to rotor turns ratio	0.3
Rated frequency	60 Hz
Stator resistance (Rs)	0.0108 pu.
Stator inductance (Ls)	0.102 pu. (referred to the stator)
Rotor resistance (Rr)	0.0121 pu.
Rotor reactance (Lr)	0.11 pu. (referred to the stator)
Mutual inductance (Lm)	3.362 pu.
Lumped inertia constant (H)	0.5 s
Dc link capacitance	39 mF
DC bus nominal voltage	1150 V
Rating of converters	0.5 pu. for each converter
Switching frequency of RSC and GSC	3 kHz

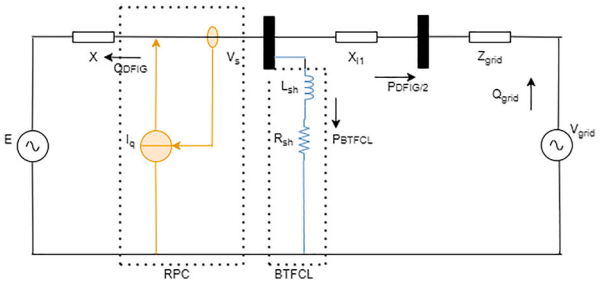

Figure 4. Equivalent circuit diagram for the cooperative operation of BTFCL and RPC during the fault.

the RSC and GSC is responsible to exchange the reactive power between the DFIG rotor and grid.

During the fault, if the fault current is more than the predefined value, BTFCL offers a very high impedance to fault current, thereby improving the stator voltage. With RPC RSC and GSC are controlled such that DIFG injects the reactive power into the grid, thereby supporting to quickly bringing the system back to its steady-state operation. So, the cooperative control of RPC and BTFCL can achieve the two main requirements of LVRT, i.e. (1) Stator voltage improvement and (2) Reactive power support.

Figure 4 shows an equivalent diagram of the basic cooperative control of BTFCL and RPC during the fault, where RPC is represented as voltage-dependent reactive current source. Controlling both converters of DFIG (RSC and GSC) can provide reactive current when the voltage of the stator (V_s) is lower than 90% of the nominal value [42]. BTFCL effectively reduces the fault current and improves the stator voltage. Thus the improved stator voltage with the help of BTFCL and RPC will support the continuous operation of DFIG during the fault, while reactive power support provided by DFIG with the help of RPC, can bring the system to its normal operating state.

4. Modelling and analysis

The mathematical model of the DFIG wind turbine connected to the grid as shown in Figure 5 is explained by deriving equations for a wound rotor induction generator, RSC and GSC. Voltage equations of stator and rotor are given by [41]

$$V_{sabc} = i_{sabc} r_s + \frac{d}{dt}\varphi_{sabc} \tag{5}$$

$$V_{rabc} = i_{rabc} r_r + \frac{d}{dt}\varphi_{rabc} \tag{6}$$

where r_s is stator resistance, r_r is the rotor resistance, v, i are voltage and current and φ is the flux linkage, subscript s stands for the stator and r stands for the rotor. Transforming the above quantities by synchronously rotating the reference frame

$$V_{ds} = i_{ds} r_s - w_s \varphi_{qs} + \frac{d}{dt}\varphi_{ds} \tag{7}$$

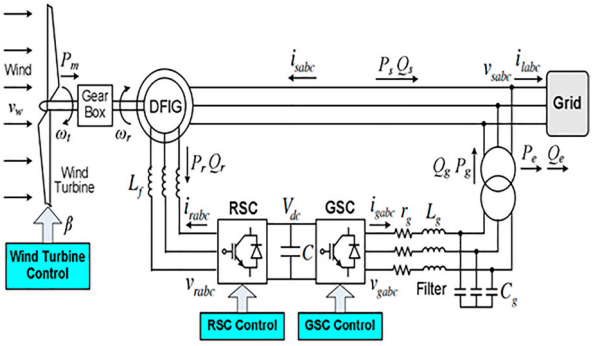

Figure 5. Schematic diagram grid-connected DFIG wind turbine [41].

$$V_{qs} = i_{qs} r_s + w_s \varphi_{ds} + \frac{d}{dt}\varphi_{qs} \tag{8}$$

$$V_{dr} = i_{dr} r_r - (w_s - w_{rr})\varphi_{qr} + \frac{d}{dt}\varphi_{dr} \tag{9}$$

$$V_{qr} = i_{qr} r_r + (w_s - w_{rr})\varphi_{dr} + \frac{d}{dt}\varphi_{qr} \tag{10}$$

where w_s is the speed of the synchronously rotating reference frame and w_{rr} is the speed of the rotor, d stands for the direct axis and q stands for the quadrature axis. Flux linkages of the machine are given by

$$\varphi_{ds} = i_{ds} L_{ls} + L_m(i_{ds} + i_{dr}) = i_{ds} L_s + i_{dr} L_m \tag{11}$$

$$\varphi_{qs} = i_{qs} L_{ls} + L_m(i_{qs} + i_{qr}) = i_{qs} L_s + i_{qr} L_m \tag{12}$$

where $L_S = L_{ls} + L_m$, L_{ls} is the stator leakage inductance and L_m is the mutual inductance.

$$\varphi_{dr} = i_{dr} L_{lr} + L_m(i_{ds} + i_{dr}) = i_{dr} L_r + i_{ds} L_m \tag{13}$$

$$\varphi_{qr} = i_{qr} L_{lr} + L_m(i_{qs} + i_{qr}) = i_{qr} L_r + i_{qs} L_m \tag{14}$$

where $L_r = L_{lr} + L_m$, L_{lr} is the rotor leakage inductance and L_m is the mutual inductance. The electromagnetic torque is given by

$$T_{em} = \varphi_{ds} i_{qs} - \varphi_{qs} i_{ds} = \varphi_{qr} i_{dr} - \varphi_{dr} i_{qr} \tag{15}$$

Substituting the above flux linkage equations in equation (15) results in

$$T_{em} = L_m(i_{dr} i_{qs} - i_{qr} i_{ds}) \tag{16}$$

By neglecting the power losses due to the stator, rotor resistance and reactance, the active and reactive powers of the rotor and stator are given by

$$P_{stator} = \frac{3}{2}(V_{ds} i_{ds} + V_{qs} i_{qs}) \tag{17}$$

$$Q_{stator} = \frac{3}{2}(V_{qs} i_{ds} - V_{ds} i_{qs}) \tag{18}$$

$$P_{rotor} = \frac{3}{2}(V_{dr} i_{dr} + V_{qr} i_{qr}) \tag{19}$$

$$Q_{rotor} = \frac{3}{2}(V_{qr} i_{dr} - V_{dr} i_{qr}) \tag{20}$$

4.1. Rotor Side Converter (RSC)

The main objective of RSC is to control the stator's real and reactive powers (P_s and Q_s) independently with effective d-axis and q-axis control loops. The control structure diagram of RSC, which is based on the stator voltage-oriented vector control method [42], is shown in Figure 6. From the control structure diagram it is observed that RSC comprises two control loops; (1) the inner current control loop and (2) the outer power control loop. The inner current control loop regulates the rotor currents $i_{dr}$and i_{qr} independently and the reference values of these currents i^*_{dr}andi^*_{qr} are obtained from the outer power control loop.

According to stator flux-oriented synchronously rotating reference frame, the direct axis is aligned with stator flux ($\varphi_{ds} = \varphi_s$ and $\varphi_{qs} = 0$). Substituting these in the above flux linkage equations (11), (12) results in the following equations

$$i_{qs} = -L_m \frac{i_{qr}}{L_s} \tag{21}$$

$$i_{ds} = L_m \frac{(i_{ks} - i_{dr})}{L_s} \tag{22}$$

$$V_{dr} = i_{dr} r_r + \alpha L_r \frac{d}{dt} i_{dr} - s w_s \alpha L_r i_{qr} \tag{23}$$

$$V_{qr} = i_{qr} r_r + \alpha L_r \frac{d}{dt} i_{qr} + s w_s \left(\alpha L_r i_{dr} + L_m^2 \frac{i_{ks}}{L_s} \right) \tag{24}$$

$$P_{stator} = \frac{3}{2}(V_{ds} i_{ds}) \tag{25}$$

$$Q_{stator} = \frac{3}{2}(-V_{ds} i_{qs}) \tag{26}$$

where S is the slip, $i_{ks} = \frac{V_{qs} - i_{qs} r_s}{w_s l_m}$ and $\alpha = 1 - \frac{L_m^2}{L_s L_r}$, by substituting of d and q axis currents and voltages in

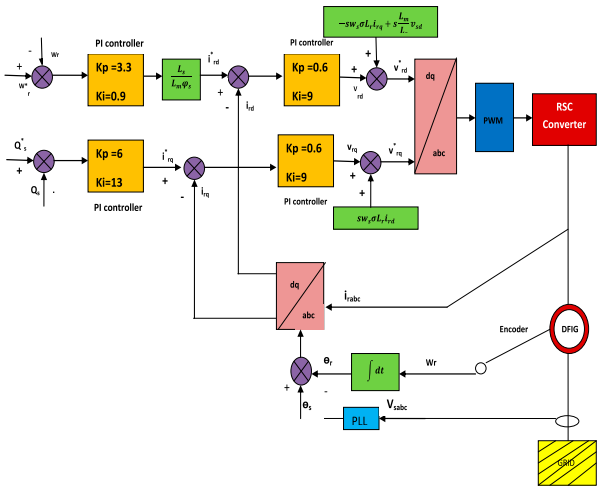

Figure 6. Control structure diagram of the Rotor Side Converter (RSC).

equations (25) and (26) results in the following

$$P_{stator} = -\frac{3}{2} \frac{w_s L_m^2 i_{ks} i_{qr}}{L_s} \tag{27}$$

$$Q_{stator} = \frac{3}{2} \frac{w_s L_m^2 i_{ks} (i_{ks} - i_{dr}) i_{qr}}{L_s} \tag{28}$$

From the above equations, it is observed that stator active and reactive powers are regulated by independent control of quadrature and direct axis rotor currents (i_{qr}, i_{dr}), the reference value of these currents is obtained from the outer power control loop. The following equations are drawn from the control structure diagram of RSC, as shown in Figure 6.

$$i^*_{dr} = \left(k_{p1} + \frac{k_{i1}}{s} \right) (w^*_r - w_r) \left(\frac{L_s}{L_m \varphi_s} \right) \tag{29}$$

$$i^*_{qr} = \left(k_{p2} + \frac{k_{i2}}{s} \right) (Q^*_s - Q_s) \tag{30}$$

$$V^*_{dr} = \left(k_{p3} + \frac{k_{i3}}{s} \right) (i^*_{dr} - i_{dr}) - s w_s \alpha L_r i_{qr} \tag{31}$$

$$V^*_{dr} = \left(k_{p4} + \frac{k_{i4}}{s} \right) (i^*_{qr} - i_{qr}) + s w_s \left(\alpha L_r i_{dr} + L_m^2 \frac{i_{ks}}{L_s} \right) \tag{32}$$

where w_r is the reference wind speed and k_p, k_i are the gains of the respective PI controller.

4.2. Grid Side Converter (GSC)

GSC can be controlled to maintain constant DC link voltage (Vdc) and to exchange the real and reactive powers with the grid.

From the block diagram of GSC, as shown in Figure 7, it is observed that, it consists of two cascaded control loops: (1) the inner current control loop and (2) the outer voltage control loop.

The active and reactive power flow from GSC to the grid, as shown in Figure 5, is expressed as follows [41]

$$P_g = \frac{3}{2}(V_{dg} i_{dg} + V_{qg} i_{qg}) \tag{33}$$

$$Q_g = \frac{3}{2}(V_{qg} i_{dg} - V_{dg} i_{qg}) \tag{34}$$

GSC ac side voltages, real and reactive powers; after applying the dq transformation and synchronously rotating reference frame where grid voltage is aligned with the d axis given by

$$P_g = \frac{3}{2}(V_{dg} i_{dg}) \tag{35}$$

$$Q_g = \frac{3}{2}(-V_{dg} i_{qg}) \tag{36}$$

$$V_{dg} = i_{dg} r_g + L_g \frac{d}{dt} i_{dg} - w_s L_g i_{qg} + V_s \tag{37}$$

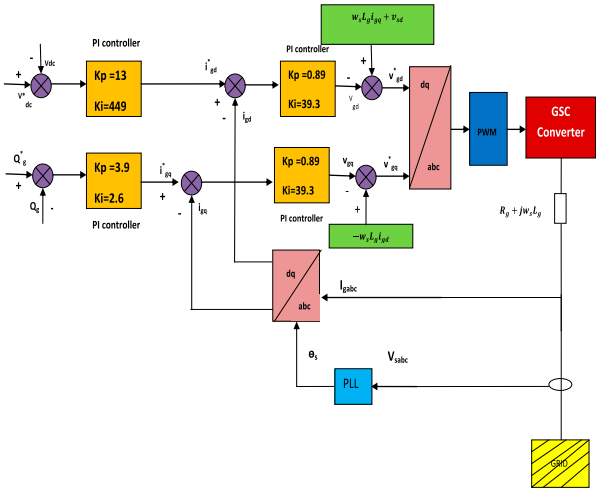

Figure 7. Control structure diagram of the Grid Side Converter (GSC).

$$V_{qg} = i_{qg} r_g + L_g \frac{d}{dt} i_{qg} + w_s L_g i_{dg} \tag{38}$$

From the above equations, it is observed that GSC maintains the constant DC link voltage by controlling i_{dg} and i_{qg}. The reference values of these currents are obtained from the outer voltage control loop and are given by

$$i^*_{dg} = \left(k_{p5} + \frac{k_{i5}}{s}\right)(V^*_{dc} - V_{dc}) \tag{39}$$

$$i^*_{qg} = \left(k_{p6} + \frac{k_{i6}}{s}\right)(Q^*_g - Q_g) \tag{40}$$

The reference voltages V^*_{dg} and V^*_{qg} are obtained from the inner current control loop and are given by

$$V^*_{dg} = \left(k_{p7} + \frac{k_{i7}}{s}\right)(i^*_{dg} - i_{dg}) - w_s L_g i_{qg} + V_s \tag{41}$$

$$V^*_{qg} = \left(k_{p8} + \frac{k_{i8}}{s}\right)(i^*_{qg} - i_{qg}) + w_s L_g i_{dg} \tag{42}$$

4.3. Reactive Power Control (RPC)

The block diagram for RPC is shown in Figure 8, during the normal operation (N) the reference reactive powers of RSC and GSC (Q^*_s and Q^*_g) are set to zero to maintain the unity power factor and to maximize the real power transfer. During the fault (F), the reference reactive powers for RSC and GSC are obtained by comparing actual and reference values of stator voltage (V_s), and then the resulting error signal is fed to the PI controller. Firstly, RSC is controlled within its available rating [39], such that DFIG injects maximum possible reactive power and then additional reactive power is injected by controlling the GSC, this is done by the reactive power output of RSC (Q_s) is one of the reactive power inputs to the GSC ($Q^*_g = Q^*_s - Q_s$). Hence the q-axis currents i^*_{qr} and i^*_{qg} must be within the current limits of RSC and GSC, respectively.

4.4. Bridge Type Fault Current Limiter (BTFCL)

BTFCL is one of the most economic solutions for fault current limiting applications because its configuration has only low-cost diodes, resistors and inductors. Compared with recent methods of using SMES and SFCL [24,25] for improving the LVRT capability, which is of very high installation cost and complex control structure, the BTFCL is the most economic and has a simple control structure [34]. The block diagram of BTFCL, as shown in Figure 9, consists of two parts (1) Shunt part with Resistance (R_{sh}) and inductance (L_{sh}) and (2) Diode part with four diodes connected to form a bridge. DC reactor with small resistance (R_{se}), inductance (L_{se}) is connected in parallel with diode and both are connected in series with the IGBT switch.

During the steady-state operation, the IGBT switch (S) is closed and current (i_{dc}) flows through $D_1 \rightarrow L_{se} \rightarrow$

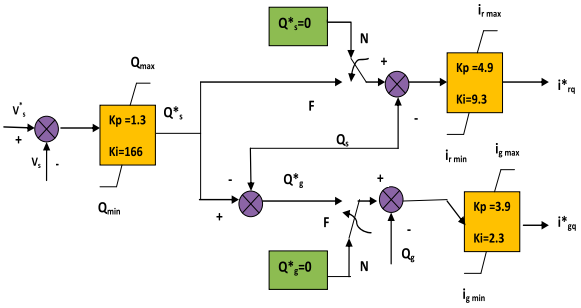

Figure 8. Control structure diagram for the Reactive Power Control (RPC).

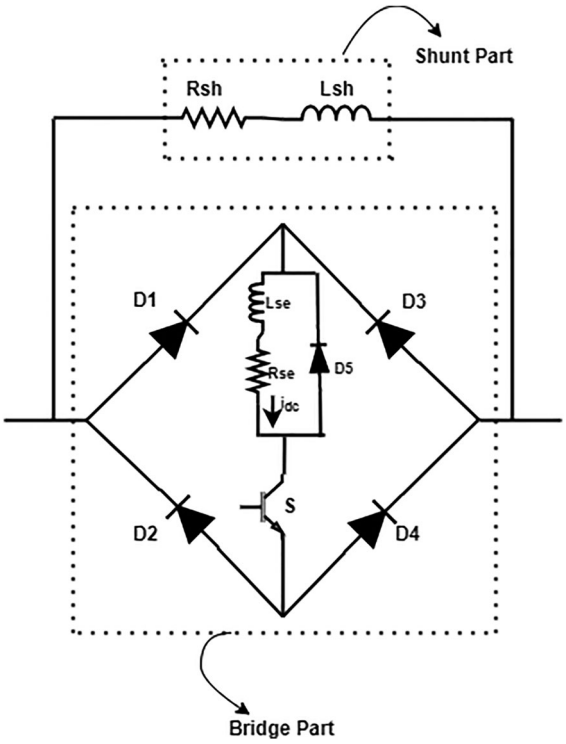

Figure 9. Schematic diagram of the Bridge-type fault current limiter.

$R_{se} \rightarrow S \rightarrow D_4$ for one-half cycles and $D_3 \rightarrow L_{se} \rightarrow R_{se} \rightarrow S \rightarrow D_2$ for another half cycle. Hence the i_{dc} flows through the L_{se} in the same direction for both cycles. During normal operation, L_{se} is charged to peak value and offers no resistance to DC (i_{dc}).

The voltage drop caused by the internal resistance of DC reactor, IGBT and diode forward voltage drop is negligible compared to line voltage drop. Hence BTFCL is more efficient in that it does not have any impact on the normal operation of DFIG and also minimum loss of power during steady-state operation.

During the fault, line current increases very rapidly but L_{se} limits the rate of rising of fault current and thereby protects the switch (S). i_{dc} is compared with the maximum permissible line current (i_{ref}), which is selected as 1.3 times of normal i_{dc} gives the optimal performance of the system under study. If i_{dc} is more than i_{ref}, the controller of BTFCL shown in Figure 10 gives the gate signals to turn off the IGBT switch. So the fault current now flows through the high resistive shunt path, thereby protecting the RSC from over current. The diode (D_5) and free-wheeling diode of IGBT provide the path for L_{se} to discharge.

After the fault is cleared, PCC voltage (V_{pcc}) will start to improve, and once it reached 90% of nominal PCC voltage (V_{ref}) the BTFCL controller forces the IGBT switch to turn on with a time delay of 1.5 cycles to avoid the current oscillations.

BTFCL controller, as shown in Figure 10, consists of two comparators: a signal accumulator and a PWM generator. The outputs of two comparators are fed through a signal control block to decide the turn-on/off status of the IGBT switch. Output from signal accumulator/control is fed through the PWM module to generate appropriate gate signal to IGBT switch (S).

4.5. Design considerations of BTFCL

The resistance and inductance of the shunt path are chosen in a way that during normal operations, the total line current flows only through the bridge part except small negligible leakage current. To expect very least disturbance near the machine during fault conditions, when the power consumed by BTFCL should be at least equal to the power carried by faulted line during normal operating conditions [34]. Power flows through the

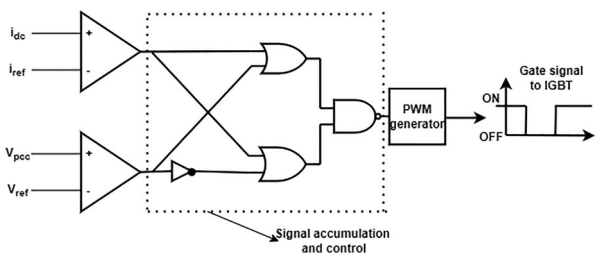

Figure 10. Bridge-Type Fault Current Limiter (BTFCL) controller.

BTFCL after the fault P_{btfcl} is given by (43) and (44)

$$P_{btfcl} \leq \frac{P_{DFIG}}{2} \tag{43}$$

$$P_{btfcl} = \frac{{V_{pcc}}^2 R_{sh}}{{R_{sh}}^2 + {X_{sh}}^2} \tag{44}$$

where P_{DFIG} is the power delivered by the machine, R_{sh} and X_{sh} are the resistance and inductance of the shunt part, respectively, and V_{pcc} is the PCC voltage.

$$R_{sh} \geq \frac{{V_{pcc}}^2 + \sqrt{({V_{pcc}}^4 - {P_{DFIG}}^2 {X_{sh}}^2)}}{P_{DFIG}} \tag{45}$$

The necessary condition for R_{sh} should be the real value and is given by

$$X_{sh} < \frac{{V_{pcc}}^2}{P_{DFIG}} \tag{46}$$

By satisfying the above equations, Table 2 shows the parameter values of BTFCL used in this study.

4.6. Designing the parameters of PI controllers

From the control structure diagram of RSC, GSC and RPC it is observed that the performance of the controller mainly depends on PI controller gains. One of the most standard methodologies used to design PI controllers is the Pole placement technique, which is based on closed-loop transfer function of the plant. In this pole placement technique, the transfer function is derived for each converter and the gains of controllers are calculated by equating characteristic equation to a second-order system. The Genetic Algorithm (GA) is used as a search engine to select the best set of gains [43].

The location of poles of closed-loop transfer function is determined by setting gains of controllers. The control loop bandwidth is defined based on the switching frequency of the respective converter. The detailed procedure of the pole placement method was discussed in [43,44] and the same is used in this study to design the PI controllers. The optimized controller gains are used for all cases of study and are shown in the respective control structure diagram of RSC (Figure 6), GSC (Figure 8) and RPC (Figure 8).

4.7. Crowbar method

The performance of the proposed method is compared with one of the most discussed methods in the literature that is crowbar resistance, as shown in Figure

Table 2. Parameters of BTFCL.

Parameter	Value
Shunt resistance (R_{sh})	0.48 pu.
Shunt inductance (L_{sh})	0.04 pu.
Series resistance (R_{se})	0.3 mΩ
Series inductance (L_{se})	1 mH

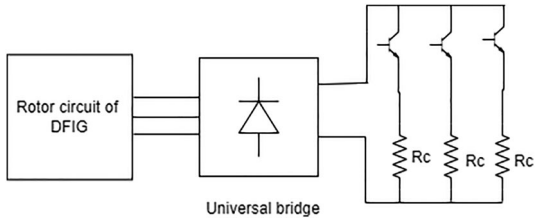

Figure 11. Block diagram of the Crowbar circuit [17].

11. It is a three-phase resistance connected in series with the rotor terminals of a DFIG through electronic switches.

During normal operations, the crowbar is not inserted into the rotor circuit. During the fault, crowbar resistance is inserted into the rotor circuit, so the entire fault current is terminated by the crowbar, thereby protecting the rotor converter from over-current and over DC link voltage. But the selection of crowbar resistance (R_c) is very critical, depending on which DFIG will draw an amount of reactive power from the grid during the fault. In this study crowbar resistance is chosen as 20 times the rotor resistance [17].

5. Simulation results and analysis

To illustrate the effects of the proposed cooperative control of BTFCL and RPC on 9 MW DFIG-based wind form, as shown in Figure 3, a test system was built and simulated in MATLAB/SIMULINK software. Simulation considerations for the test case are as follows: the most severe fault on a power system i.e. Triple line to ground (LLLG) fault is applied at one of the critical points F_1 at 1 s for the duration of 150 ms. Circuit breakers CB_1 and CB_2 on the transmission line (T_{r2}) are opened at 1.1 s and successfully re-closed at 1.65 s. The performance of the machine is analyzed by studying the following quantities from the simulation results.

5.1. Reactive power

With crowbar there is no reactive power support from DFIG, instead of that DFIG is absorbing the 0.14 Mvar reactive power from the grid, as shown in Figure 14. With BTFCL alone also DFIG does not provide any reactive power support to the grid. Using RPC alone, DFIG can produce 1.059 pu reactive current i.e. with controlling GSC, DFIG can produce 0.216 pu and with controlling RSC, DFIG can produce 0.843 pu as shown in Figure 12 and Figure 13. Reactive power produced by DFIG with the help of RPC alone is 0.73 Mvar, as shown in Figure 14. But with the proposed method of cooperative control of BTFCL and RPC, the DFIG can inject 1.5 Mvar reactive power into the grid during the fault, as shown in Figure 14.

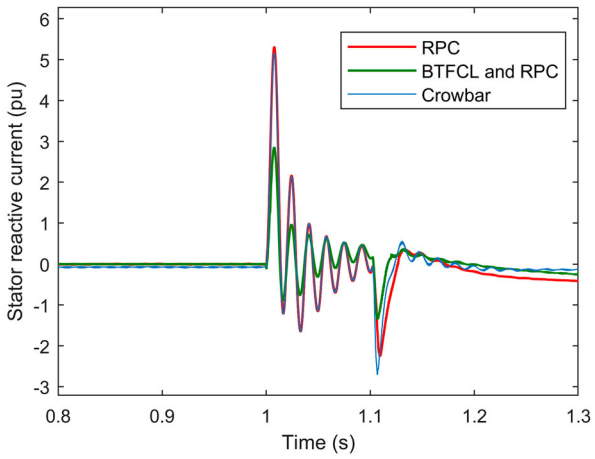

Figure 12. Reactive current from the rotor side converter.

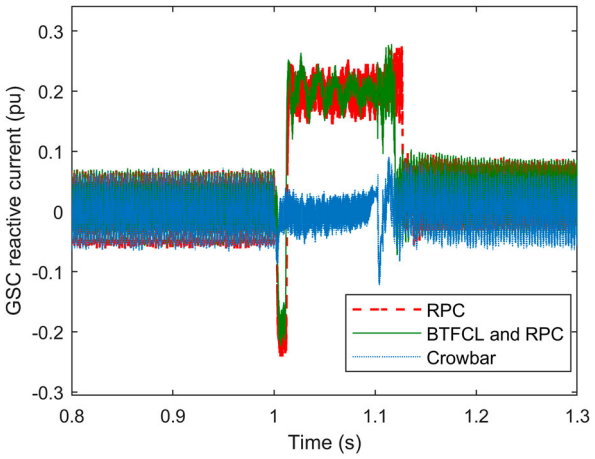

Figure 13. Reactive current from the grid side converter.

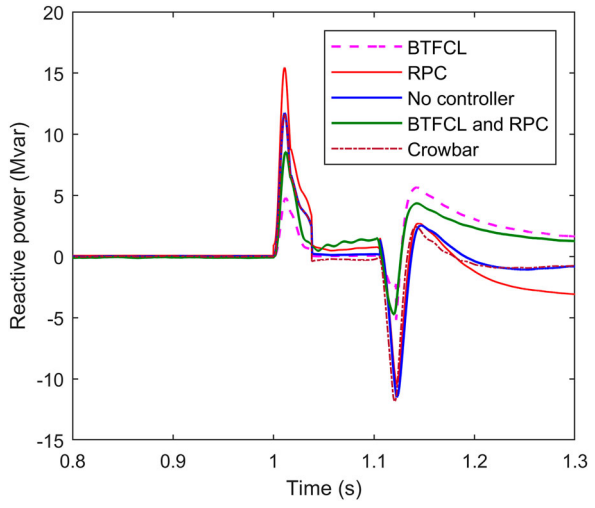

Figure 14. Reactive power produced by DFIG with different controls.

5.2. Stator voltage

From Figure 15, it is observed that conventional crowbar resistance results in no improvement in the stator voltage V_s and with RPC alone, the stator voltage is improved from 55 V to 62 V. With the acting of BTFCL

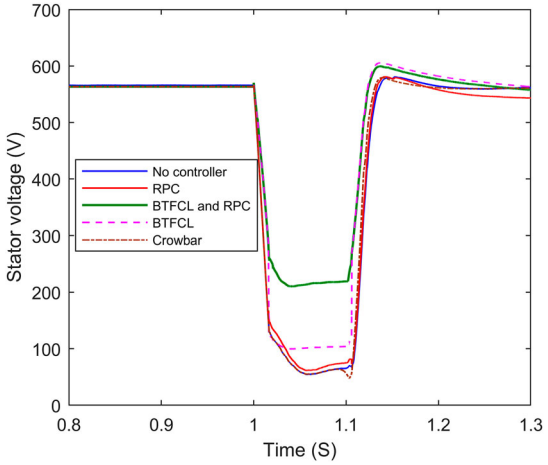

Figure 15. Stator voltage of DFIG with different controls.

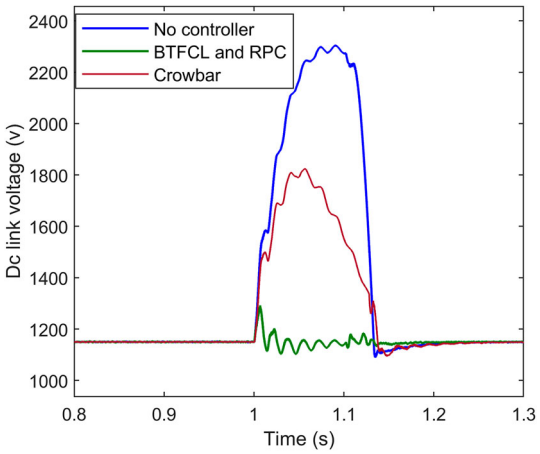

Figure 16. DC link voltage of DFIG with different controls.

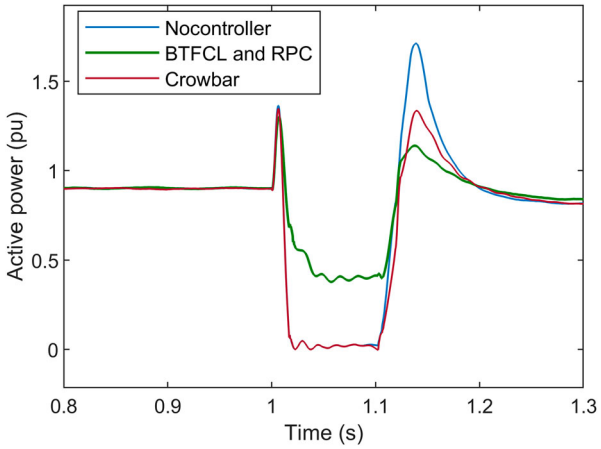

Figure 17. Electromagnetic torque profile of DFIG with different controls.

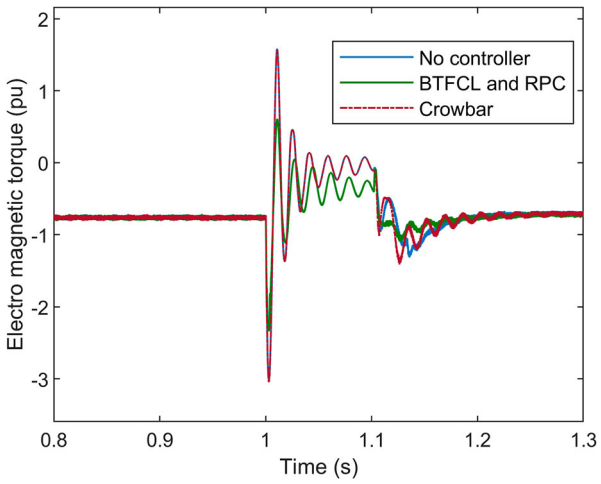

Figure 18. Active power from DFIG with different controls.

alone, the stator voltage is improved to 100 V. But with the proposed method of cooperative control of BTFCL and RPC would result in the stator voltage increased to 220 V, thereby strictly satisfying the grid code requirements [36].

5.3. DC link voltage

With LLLG fault, the DC link voltage of DFIG is increased from 1150 V to 2300 V, as shown in Figure 16, which may damage the IGBT converters of rated voltage 1700 V. With crowbar resistance, the DC link voltage is limited to 1820 V and is not in the safe operating limits, but with proposed cooperative control, the DC link voltage is maintained at 1180 V, which is within safe operating limits.

5.4. Electromagnetic torque

Figure 17 shows the electromagnetic torque profile, without any controller the oscillations are very high, which may reduce the lifetime of the gearbox and turbine shaft. The torque oscillations with the crowbar method are still very high. With the proposed control, the oscillations are reduced to one-fourth of the previous case, thereby protecting the system.

5.5. Active power

With a rated wind speed of 15 m/s, the DFIG wind plant can produce 0.9 pu active power, as shown in Figure 18 during the steady-state operation. During the fault, with the crowbar method, the active power produced by DFIG becomes nearly zero, but with the proposed control, this value is increased to 0.4 pu. From Figure 18, it is observed that at the instant of fault clearance the active power demand on the machine increased to a very high value, which is harmful to the machine without any protection. But with the proposed control this fluctuation is very low with normal operating demand on the machine, thereby reducing the stress on the turbine generator system.

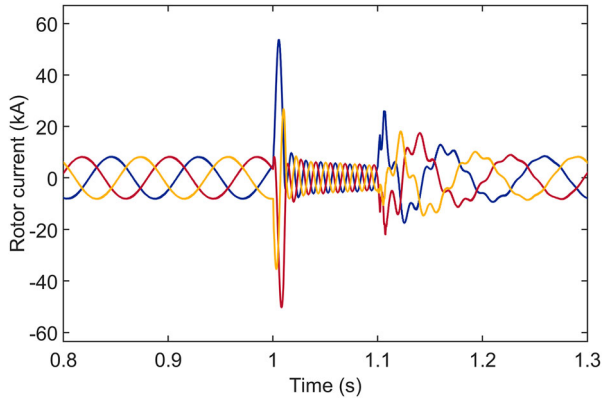

Figure 20. Fault current through the rotor circuit of DFIG with crowbar control.

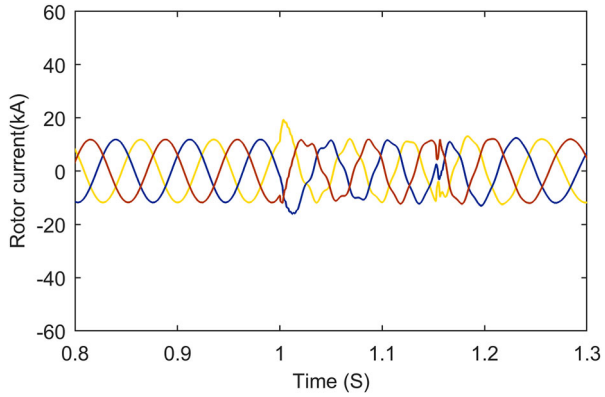

Figure 21. Fault current through the rotor circuit of DFIG with the proposed control.

5.6. Rotor current

Fault current through the DFIG rotor circuit for typical LLLG is shown in Figure 19. From the figure, it is observed that a very high magnitude of fault current i.e. 19.6 kA flowing through the rotor circuit during the fault, can damage the power electronic converters, if without any proper protection. Fault current through the rotor circuit is much limited to 7.8 kA using the crowbar resistance shown in Figure 20. With the proposed control technique fault, the current is reduced to 4.6 kA, as shown in Figure 21, which is well below the maximum current rating of converters, thereby protecting the RSC.

Table 3. Comparison of different methods on DFIG when subjected to symmetrical fault.

Quantity	No control	Crowbar	RPC	BTFCL	Proposed method
Reactive power (Mvar)	0	−0.14	0.73	0	1.5
Stator voltage (V)	55	57	62	100	220
Rotor current (kA)	19.6	7.8	12.3	6.1	4.6
Dc link voltage (kV)	2.3	1.7	2.0	1.26	1.18

From the simulation results, it is observed that the conventional method of using a crowbar can only limit rotor over-current and DC link voltage during the fault. But there is no reactive power support and no improvement in stator voltage; hence, this method is not able to meet the two main objectives of LVRT capability. But with the proposed method, the fault current through the rotor circuit and DC link voltage is well limited and the stator voltage is improved and DFIG can provide reactive power support to the grid. Hence the cooperative control of BTFCL and RPC can efficiently enhance the LVRT capability of grid-connected DFIG compared with the crowbar method. A comparison of the performance of different protection methods on DFIG wind farm when subjected to LLLG fault is given in Table 3.

6. Conclusion

Cooperative control of BTFCL and RPC has been proposed in this study to enhance the LVRT capability

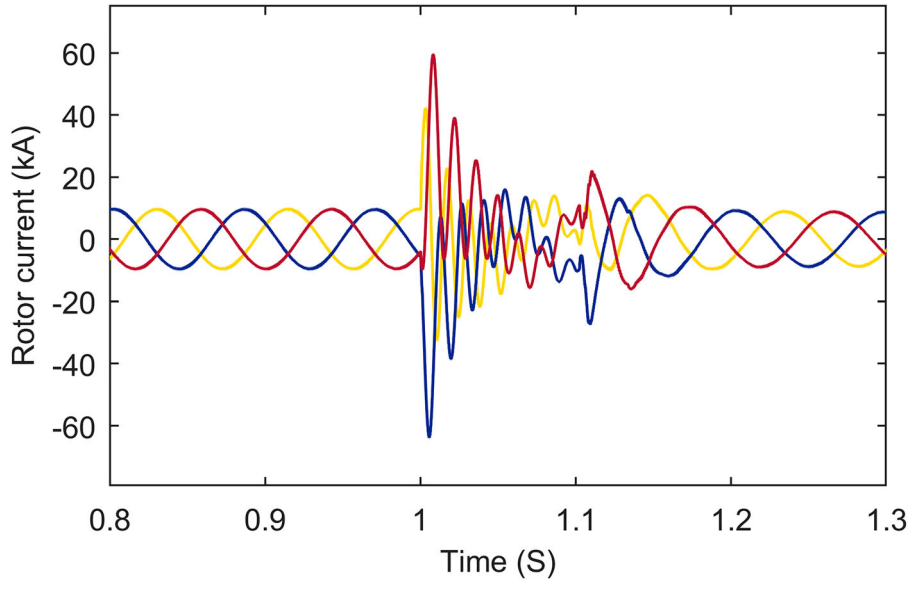

Figure 19. Fault current through the rotor circuit of DFIG without any control.

of a 9 MW DFIG-based wind plant. The importance of LVRT requirements, basic principles, detailed system modelling and simulation results are analyzed and explained in detail. The simulation results show that

- Only with BTFCL, the fault current is effectively reduced and minimum PCC voltage is improved with no reactive power support.
- With simple RPC, DFIG provides reactive power support to the grid with very low improvement in PCC voltage.
- By the combined control of BTFCL and RPC, PCC voltage is improved more than the required value by new grid codes and thereby supporting the machine to continue its operation with the grid during the fault for a specific period. Secondly, with this cooperative control DFIG can provide reactive power support to the grid to quickly bring back the system to its steady-state operation.

The proposed method of improving LVRT capability is strictly satisfying the new grid codes and it is the most efficient, economic and reliable method to achieve the two main requirements of LVRT compared with the conventional crowbar resistance method.

Acknowledgment

Authors would like to thank Anna University for providing Anna Centenary Research Fellowship to support this research work.

Disclosure statement

No potential conflict of interest was reported by the author(s).

ORCID

K. Gireeshma http://orcid.org/0000-0002-6641-4658
S. Chandramohan http://orcid.org/0000-0001-6016-307X

References

[1] https://iea.blob.core.windows.net/The_role_of_CCUS_in_low-carbon_power_systems.pdf.
[2] https://gwec.net/global-wind-report-2021/.
[3] https://www.gwec.net/wp-content/uploads/2013/06/GWEC_global_fact_sheets.pdf.
[4] Sourkounis C, Tourou P. Grid code requirements for wind power integration in Europe. Conf Pap Sci. 2013: 1–9. DOI:10.1155/2013/437674.
[5] Eltamaly AM, Al-Saud MS, Abo-Khalil AG. Dynamic control of a DFIG wind power generation system to mitigate unbalanced grid voltage. IEEE Access. 2020;8:39091–39103. DOI:10.1109/ACCESS.2020.2976195.
[6] Mahela OP, Gupta N, Khosravy M, et al. Comprehensive overview of low voltage ride through methods of grid integrated wind generator. IEEE Access. 2019;7:99299–99326. DOI:10.1109/ACCESS.2019.2930413.
[7] Rini Ann Jerin A, Kaliannan P, Subramaniam U, et al. Review on FRT solutions for improving transient stability in DFIG-WTs. IET Renew Power Gener. 2018;12:1786–1799. DOI:10.1049/iet-rpg.2018.5249.
[8] Ayyarao TSLV. Modified vector controlled DFIG wind energy system based on barrier function adaptive sliding mode control. Prot Control Mod Power Syst. 2019;4; DOI:10.1186/s41601-019-0119-3.
[9] Zhu R, Chen Z, Wu X, et al. Virtual damping flux-based LVRT control for DFIG-based wind turbine. IEEE Trans Energy Convers. June 2015;30(2):714–725. DOI:10.1109/TEC.2014.2385966.
[10] Zhu R, Chen Z, Tang Y, et al. Dual-loop control strategy for DFIG-based wind turbines under grid voltage disturbances. IEEE Trans Power Electron. March 2016;31(3):2239–2253. DOI:10.1109/TPEL.2015.2442520.
[11] Zhu D, Zou X, Zhou S, et al. Feedforward current references control for DFIG-based wind turbine to improve transient control performance during grid faults. IEEE Trans Energy Convers. June 2018;33(2):670–681. DOI:10.1109/TEC.2017.2779864.
[12] Park G, Kim J, Kang YC. Transient voltage control of a DFIG-based wind power plant for suppressing overvoltage using a reactive current reduction loop. J Int Coun Elect Eng. 2016;6(1):140–145. DOI:10.1080/22348972.2016.1189809.
[13] Rafiee Z, Rafiee M, Aghamohammadi R. Improvement of transient voltage profile using power control of the DFIG-based wind farm under severe voltage dip event. IJEEE. 2020;16(3):313–324.
[14] Ghosh S, Isbeih YJ, Bhattarai R, et al. A dynamic coordination control architecture for reactive power capability enhancement of the DFIG-based wind power generation. IEEE Trans Power Syst. 2020;35(4):3051–3064. DOI:10.1109/TPWRS.2020.2968483.
[15] Jabbour N, Tsioumas E, Mademlis C, et al. A highly effective fault-ride-through strategy for a wind energy conversion system with a doubly fed induction generator. IEEE Trans Power Electron. 2020;35(8):8154–8164. DOI:10.1109/TPEL.2020.2967971.
[16] Noureldeen O, Hamdan I. A novel controllable crowbar based on fault type protection technique for DFIG wind energy conversion system using adaptive neuro-fuzzy inference system. Prot Control Mod Power Syst. 2018;35(3):1–12. DOI:10.1186/s41601-018-0106-0.
[17] Ibrahim NZ, Al-Quteimat A, et al. A novel approach for crowbar resistance determination for doubly fed induction generators in wind energy conversion systems. Int J Amb Energy. 2021: 1–22. DOI:10.1080/01430750.2021.1874519.
[18] QU Y, GAO, L, MA, G. et al. Crowbar resistance value-switching scheme conjoint analysis based on statistical sampling for LVRT of DFIG. J Mod Power Syst Clean Energy. 2019;7:558–567. DOI:10.1007/s40565-018-0444-y.
[19] Jiang H, Zhang C, Zhou T, et al. An adaptive control strategy of crowbar for the low voltage ride-through capability enhancement of DFIG. Energy Proc. 2019;158:601–606. DOI:10.1016/j.egypro.2019.01.161.
[20] Naderi SB, Negnevitsky M, Muttaqi KM. A modified DC chopper for limiting the fault current and controlling the DC-link voltage to enhance fault ride-through capability of doubly-fed induction-generator-based wind turbine. IEEE Trans Indus Appl. April 2019;55(2):2021–2032. DOI:10.1109/TIA.2018.2877400.

[21] Hossain Md E. Low voltage ride-through capability improvement methods for DFIG based wind farm. J Electr Syst Inform Technol. 2018;5(3):550–561. doi: 10.1016/j.jesit.2017.12.002.
[22] Zhang D, Xu H, Qiao L, et al. LVRT capability enhancement of DFIG based wind turbine with coordination control of dynamic voltage restorer and inductive fault current limiter. PLoS One. August 2019;14(8), DOI:10.1371/journal.pone.0221410.
[23] Mukherjee P, Rao VV. Superconducting magnetic energy storage for stabilizing grid integrated with wind power generation systems. J Mod Power Syst Clean Energy. 2019;7:400–411. DOI:10.1007/s40565-018-0460-y.
[24] Ngamroo I, Karaipoom T. Cooperative control of SFCL and SMES for enhancing fault ride through capability and smoothing power fluctuation of DFIG wind farm. IEEE Trans Appl. Supercond. 2014;24(5):1–4. DOI:10.1109/TASC.2014.2340445.
[25] Sahoo S, Mishra A. (2017). Enhanced fault ride – through ability of DFIG-based wind energy system using superconducting fault current limiter. 4th International Conference on Power, Control & Embedded Systems (ICPCES), 1–5. DOI:10.1109/ICPCES.2017.8117627.
[26] Zou Z, Chen X, Li C, et al. Conceptual design and evaluation of a resistive-type SFCL for efficient fault ride through in a DFIG. IEEE Trans Appl Supercond. 2016;26(1):1–9. DOI:10.1109/TASC.2015.2507129.
[27] Musarrat MN, Fekih A, Islam MR. An improved fault ride through scheme and control strategy for DFIG-based wind energy systems. IEEE Trans Appl Supercond. 2021;31(8):1–6. DOI:10.1109/TASC.2021.3096181.
[28] Yang RH, Jin JX. Unified power quality conditioner with advanced dual control for performance improvement of DFIG-based wind farm. IEEE Trans Sustain Energy. 2021;12(1):116–126. DOI:10.1109/TSTE.2020.2985161.
[29] Chen L, Li G, Chen H. Combined use of a resistive SFCL and DC-link regulation of a SMES for FRT enhancement of a DFIG wind turbine under different faults. IEEE Trans Appl Supercond. 2019;29(2):1–8. DOI:10.1109/TASC.2018.2881988.
[30] Du KJ, Ma XP, Zheng ZX, et al. LVRT capability improvement of DFIG-based wind turbines with a modified bridge-resistive-type SFCL. IEEE Trans Appl Supercond. 2021;31(8):1–5. DOI:10.1109/TASC.2021.3091114.
[31] Naderi SB, Jafari M. Impact of bridge type fault current limiter on power system. Proc 7th Int Conf Elect Electron Eng. 2011: 1–4.
[32] Ghanbari T, Farjah E, Tashakor N. Thyristor based bridge-type fault current limiter for fault currentlimiting capability enhancement. IET Gener Transm Distrib. 2016;10:2202–2215. DOI:10.1049/iet-gtd.2015.1364.
[33] Padmaja A, Shanmukh A, Mendu SS, et al. Design of capacitive bridge fault current limiter for low-voltage ride-through capacity enrichment of doubly fed induction generator-based wind farm. Sustainability. 2021;13(12):6656. DOI:10.3390/su13126656.
[34] Rashid G, Ali MH. Transient stability enhancement of doubly fed induction machine-based wind generator by bridge-type fault current limiter. IEEE Trans Energy Convers. 2015;30(3):939–947. DOI:10.1109/TEC.2015.2400220.
[35] https://gwec.net/wind-could-supply-20-of-global-power-by-2030-gwec/.
[36] Tsili M, Papathanassiou S. A review of grid code technical requirements for wind farms. IET Renew Power Gene. 2009;3(3):308–332. DOI:10.1049/iet-rpg.2008.0070.
[37] Zhai J, Liu H. Reactive power control strategy of DFIG wind farms for regulating voltage of power grid. IEEE PES Gener Meet Conf Expos. 2014: 1–5. DOI:10.1109/PESGM.2014.6939441.
[38] Weng Y, Hsu Y. Reactive power control strategy for a wind farm with DFIG. Renew Energy. 2016;94:383–390. DOI:10.1016/j.renene.2016.03.072.
[39] Kasem AH, El-Saadany EF, El-Tamaly HH, et al. An improved fault ride-through strategy for doubly fed induction generator-based wind turbines. IET Renew Power Gener. 2008;2(4):201–214. DOI:10.1049/iet-rpg:20070092.
[40] Shen Y, Cui M, Wang Q, et al. Comprehensive reactive power support of DFIG adapted to different depth of voltage sags. Energies. 2017;10(6):808. DOI:10.3390/en10060808.
[41] Qiao W. Dynamic modeling and control of doubly fed induction generators driven by wind turbines. IEEE PES Power Syst Conf Expos. 2009: 1–8. DOI:10.1109/PSCE.2009.4840245.
[42] Ou R, Xiao XY, Zou ZC, et al. Cooperative control of SFCL and reactive power for improving the transient voltage stability of grid-connected wind farm with DFIGs. IEEE Trans Appl Supercond. 2016;26(7):1–6. DOI:10.1109/TASC.2016.2574344.
[43] Vieira JP, Nunes MV, Bezerra UH. Designing optimal controllers for doubly fed induction generators using a genetic algorithm. IET Gener Trans Distrib. 2009;3(5):472–484. DOI:10.1049/iet-gtd.2008.0239.
[44] Yang L, Yang GY, Xu Z, et al. Optimal controller design of a doubly-fed induction generator wind turbine system for small signal stability enhancement. IET Gener Trans Distrib. 2010;4(5):579–597. DOI:10.1049/iet-gtd.2009.0553.